HAL
open science

Crustal thickness in Vrancea area, Romania from S to P converted waves

Marian Ivan

To cite this version:

Marian Ivan. Crustal thickness in Vrancea area, Romania from S to P converted waves. Journal of Seismology, 2011, 15 (2), pp.317-328. 10.1007/s10950-010-9225-4 . hal-00659892

HAL Id: hal-00659892

https://hal.science/hal-00659892v1

Submitted on 14 Jan 2012

HAL is a multi-disciplinary open access archive for the deposit and dissemination of scientific research documents, whether they are published or not. The documents may come from teaching and research institutions in France or abroad, or from public or private research centers.

L'archive ouverte pluridisciplinaire **HAL**, est destinée au dépôt et à la diffusion de documents scientifiques de niveau recherche, publiés ou non, émanant des établissements d'enseignement et de recherche français ou étrangers, des laboratoires publics ou privés.

Manuscript
Click here to download Manuscript: Ivan_rev1.doc
Click here to view linked References

Crustal thickness in Vrancea area-Romania from S to P converted waves

Marian Ivan

Department of Geophysics, University of Bucharest, 6 Traian Vuia str., 020956 Bucharest o.p.37, Romania

National Institute of Earth Physics, P.O.Box MG-21, Bucharest-Magurele, Romania

FAX: 0040212113120

marian.ivan@g.unibuc.ro

Crustal thickness (CT) in Vrancea region (Romania) and adjacent area is investigated using 1294 S to P converted waves from the Moho discontinuity. A total of 269 local earthquakes in the depth range 99.8 to 171.1 km and recorded by 76 permanent and 46 temporary stations of the Romanian Seismological Network are used. Time difference between the converted wave and the direct P phase is corrected to a first order for epicentral distance and for the errors in focal depth, being finally inverted to CT. Greatest values for the Moho depth are observed for stations located in the Carpathians molasse foredeep and smaller values are observed in the Southern part of the Moesian Platform, for stations in the eastern part of Moldavian (East-European) Platform and in Dobrogea area, close to the Black Sea shoreline. In Vrancea epicentral area, an important CT variation is observed, from 42 km at MLR and 41.8 km at SIR, stations placed in the south-western part of the epicentral area, to 30.9 km at VRI, located above north-eastern part of the seismogenic volume. Stations CVO and OZU, placed in Transylvanian Basin in the proximity of the epicentral area, have CT values of 32.1 and 24.1 km, respectively. The results seem to support that a mantle delamination process is responsible for Vrancea intermediate depth seismicity.

S to P converted waves, crustal thickness, Vrancea (Romania)

1 Introduction

Vrancea zone is one of the most active intra-continental seismic areas in Europe (Fig. 1), with potential seismic hazard associated to a few intermediate depth earthquakes (1940, November, 10th, Mw=7.7, H=150 km; 1977, March, 3rd, Mw=7.4, H=94 km; 1986, August, 30th, Mw=7.1, H=131 km; 1990, May, 30th, Mw=6.9, H= 91 km; 1990, May, 31st, Mw=6.4, H=87 km). Surrounding Vrancea, the stations of the Romanian Seismic Network (Fig. 2) are placed in different tectonic units, i.e. Moldavian (East-European) Platform, Carpathian Arc and Moesian Platform. Attempts to explain the Vrancea seismicity cover almost the whole range of the actual existing geodynamic scenarios (see a synopsis in Mucuta et al. 2006). However, both the nature of the sub-crustal seismic activity,

which is confined to a near vertical volume, and the fine details tectonic structure in Vrancea and adjacent area are still open to various scientific debates (Milsom 2005). Frequently, a conspicuous phase located between P and S (Fig. 3) can be observed for events exceeding 100 km depth and recorded at epicentral distances less than 2°. The arrival time, particle motion and the frequency content (which is, at least in several cases, also intermediate between P and S) suggest that phase to be a S wave converted and transmitted as P on the Moho discontinuity (e.g. Båth and Stefánsson 1966; Smith 1970). It is best observed at stations projected in the proximity of a nodal plane on the focal hemisphere, as it is also suggested by the relative amplitude ratios on synthetic seismograms obtained by the reflectivity method (Wang 1999). Such converted phases have been extensively observed in various regions of the world and used to map the lithosphere-astenosphere boundary (Sacks and Snoke 1977), the crustal thickness (Regnier et al. 1994; Narcía-López et al. 2004), the location of the upper slab-astenosphere interface (Nakamura et al. 1998), or the geometry of the upper boundary of the plates (Ohmi and Hori 2000). In this paper, the time difference between the converted phase (sp) and the direct p wave is corrected to a first order for epicentral distance and for the event depth by using the local velocity model (LVM) routinely used in earthquake location by the Romanian National Institute for Earth Physics (NIEP) (Oncescu 1984). By using a method to minimize the errors in focal depth, the corrected time difference values (sp - p) are inverted to evaluate the crustal thickness in (proximity of) Vrancea. The CT values are finally compared to the previous results provided by active seismic experiments in the area, by the receiver function analysis, by the inversion of the surface waves and to the values suggested by the astronomic quasi-geoid heights map.

2 Method

Let t_{ij} be the observed minus computed (O-C) difference between the arrival of the converted sp phase and the direct P wave, manually picked at the j-th station for the i-th earthquake

$$t_{ij} = t_{sp}^{O} - t_{p}^{O} - \left(t_{sp}^{C} - t_{p}^{C}\right) \qquad (1)$$

Especially for small epicentral distances, the errors in focal depth (routinely around 10-15 km) are shifting the computed sp-P time difference by a near

constant value C_i, which is approximately the same for all the recording stations (Fig. 4). Hence, to a first order, the difference

$$t_j = t_{ij} - C_i \qquad (2)$$

will be a characteristic of each j-th station, depending mainly on the Moho depth beneath the recording station. It can be evaluated from a weighted least-squared minimum

$$\sum_{i=1}^{NE}\sum_{j=1}^{NS} w_{ij}\left(t_{ij} - t_j - C_i\right)^2 = \min \quad , (3)$$

where w_{ij} are the values of the weights, NE is the total number of earthquakes and NS is the total number of stations which recorded a certain i-th event. Vanishing the first-order partial derivatives of (3) with respect to C_i and t_j, it follows the unknown values of t_j are obtained by solving the linear system

$$\sum_{k=1}^{NS} a_{jk} t_k = b_j \quad , \text{k,j=1,…,NS} , (4)$$

with

$$a_{jk} = \sum_{i=1}^{NE} w_{ik}\left(\delta_{kj} - w_{ik} / \sum_{l=1}^{NS} w_{il}\right) \qquad (5)$$

and

$$b_j = \sum_{i=1}^{NE} w_{ij}\left(t_{ij} - \sum_{l=1}^{NS} w_{il} t_{il} / \sum_{l=1}^{NS} w_{il}\right) , (6)$$

where δ_{kj} is Kronecker's symbol.

The value of t_j has been assumed to be the same for stations with close location and/or in very similar tectonic settings. In such case, a representative station located in the proximity of the centroid of the whole group has been selected. For each (group of) station(s), an average earthquake location was evaluated. Its coordinates is the arithmetic mean of latitudes, longitudes and depth values of all the events recorded by that (group) of station(s) (Table 1). Piercing points to Moho of p and sp waves were obtained for every (representative) station and for

the corresponding average earthquake using the LVM with the Moho depth at 40 km. The values of t_j were interpolated with the minimum curvature method in a grid of 81 (latitude) by 100 (longitude) cells, being assigned to the mid-point between p and sp piercing points. For every (representative) station and corresponding average event, the value of t_j was converted to Moho depth (M_d) by a trial and error method. The value of 40 kms assigned to M_d into the LVM and used in (1) was slightly modified until t_j value was reached. All the other parameters of the LVM remain unchanged. For the 52 (representative) stations (Table1), there is a linear correlation between the evaluated Moho depth and t_j values (Fig. 5) which was used to obtain M_d for the rest of the grid points.

3 Data collection

Three sources of digital waveforms available at NIEP Data Center have been used in this study. The first one is represented by the recordings of the Geotech S-13 network (white triangles in Figure 2) during 1982-1997, which produced 61 earthquakes for the analysis. That network had a 50 Hz sampling and a common time base for all the stations (most of them being equipped with vertical sensors only). A second source, which provided 186 events for the period 1997-2007, June 30th, is the K2 network (Bonjer et al. 2000) (black triangles in Figure 2), with a variety 3-component instruments at 200 Hz sampling and individual GPS timing. The third source was Calixto 99 experiment (Figure 6) which provided another 22 events. Several waveforms have been obtained also from GFZ Data Center, for the Romanian broad-band stations. All the existing recordings have been checked for the presence of conspicuous P and sp converted phases. In each case, a weight (good, fair and poor) has been ascribed to each sp / p reading, depending on the signal to noise ratio and to the presence of signal on both vertical and radial channels (where available). Only earthquakes showing sp phases at two or more stations (at least one of them with fair or good weight) have been selected and processed according to eq.(1)-(6). The computed values have been evaluated using TauP Toolkit (Crotwell et al. 1999) for the LVM having the Moho depth at 40 km (Oncescu 1984). Event locations are provided by the updated Romplus catalogue (Oncescu et al. 1999).

3 Results and discussion

The above estimations of Moho depth have been compared to the results obtained in the area from receiver function analysis (Diehl et al. 2005; Geissler et al. 2008; Tãtaru 2009). The values in Table 2 suggest that the errors in the Moho depth estimations in this study are around ±3 kms, with a noticeable difference at station E25 where the difference is around 10 km. There is a good agreement too in respect to the Moho depth at shot points G, H, K, L and M of the controlled seismic experiment VRANCEA99 (Hauser et al. 2001). For the shot points D, E, F, R, S, T (VRANCEA99, VRANCEA2001), the Moho depth estimated from sp conversions seems to be underestimated by around 7-8 km. The discrepancies could be due to lateral variations of P wave velocity, especially in the crust, or a failure of the interpolation technique. The minimum curvature method is assuming a continuous, smooth geometry of a thin elastic plate (e.g. Briggs, 1974), which could not be valid in the presence of a few crustal faults (see Fig. 1). Furthermore, most observations at CFR station (which provided the Moho depth in the area of shot points R and S) are of low quality, especially because the arrival of P wave at that station is routinely difficult to be identified accurately.

Greatest negative values of t_j are obtained in Carpathians mollasse for-deep and Focsani Basin, similar to the features suggested by the quasi-geoid heights (Fig. 2). The geodetic values are related to the variations of the Newtonian potential on the Earth surface, mostly as a result of both density contrast between the crust / upper mantle, and to the Moho topography. In the southern part of the investigated area (proximity of Bucharest city), a clear increase of the t_j values is observed from North to South, suggesting a decrease of crustal thickness toward Danube. This feature is in agreement to the results provided by surface wave dispersion (Raykova and Panza 2006). In the Eastern most part of the Figure 7, t_j values are decreasing from East to West, possibly because of the presence of a crust fault (the Danube fault), approximately located along the longitude of 27.5°-28°E, between latitude 44 and 45° N (see also the tomographic results of Fan et al. (1998)). The t_j values in Vrancea epicentral area indicate a strong lateral variation of crustal thickness. At MLR and SIR, located in the south-western part of the epicentral area, CT values are around 42 kms. At VRI station, located

above north-eastern part of the seismogenic volume, CT value is around 31 km. An important variation of attenuation have been reported here by Ivan (2007). Stations CVO and OZU, located in Transylvanian Basin in the proximity of the epicentral area, have CT values of 32.1 and 24 km, respectively, in agreement to the value around 27.5 at the temporary station S07 of CALIXTO99 experiment (Diehl, 2005) and to Raykova and Panza (2006) observations in cell 15 f (28.5-33.5 km). However, shot points U and W (VRANCEA2001 experiment) provided here a Moho depth around 34 km and a strong reflector around 27 km depth has been assumed to represent a limit separating the middle / lower crust by Hauser et al. (2007).

Converted phases can be also used to provide an estimation of focal depth. For example, the value of C_i in eq.(2) for the 2005/04/04 event (Figure 3) is –2.07 seconds. It suggests that the assumed depth of 141 km (Romplus catalogue) is overestimated by around 20 km (see Figure 4), in agreement with the depth provided by other agencies (i.e. 120 km / SOF /, 121.1 km / CSEM / and 115.5f / NEIC /)(see details in ISC Catalogue). Considering the observations in Figure 8 and the LVM with the Moho depth at 40 km, the rms values for (O-C) sp-p time differences are 2.45 s (for the focal depth at 141 km) and 0.77 s (for h=121 km). The rms value is further decreased to 0.53 s for the LVM with variable Moho depth and h=121 km.

4 Conclusions

Converted waves appear to be an useful tool for investigating crustal thickness in Vrancea and adjacent areas. Most results are in good agreement to the values derived by various techniques (receiver function, active seismic experiments, surface wave dispersion). Proper identification of the converted sp phase can improve the accuracy of intermediate depth event location (especially the focal depth), better constraining the focal mechanism too. Including such waves into local tomographic investigations can substantially improve the resolution of the derived models. The thin crust obtained from converted phases in the epicentral area might support the mantle delamination as a possible geodynamic mechanism for Vrancea seismicity (e.g. Gîrbacea and Frisch 1998; Sperner et al. 2001; Gvirtzman 2002; Knap et al. 2005; Fillerup et al., 2010).

Acknowledgements

This research has been partially supported by ANCS grant D11-025/15.09.2007. Romanian Military Topographic Department is highly acknowledged for the permission to present the quasi-

geoid data. GFZ Potsdam is acknowledged for maintaining the Data Archive. GMT files (Wessel & Smith 1996) have been used to prepare some of the diagrams. The author is grateful to Dr. Rongjiang Wang (GFZ Potsdam) for making the reflectivity method code available. Comments and suggestions of Dr. Jiri Zahradnik and two anonymous referees definitely improved the manuscript.

References

Båth M, Stefánsson R (1966) S-P conversion at the base of the crust. Annali Geofis XIX: 119-130

Bonjer K-P, Oncescu MC, Rizescu M, Enescu D, Driad L, Radulian M, Ionescu C, Moldoveanu T (2000) Source- and site-parameters of the April 28, 1999 intermediate depth Vrancea earthquake: First results from the new K2 network in Romania, XXVII General Assembly of the European Seismological Commission, Lisbon, Portugal, Book of Abstracts and Papers, SSA-2-13-O 53

Briggs IC (1974) Machine contouring using minimum curvature. Geophysics 39:39-48

Crotwell HP, Owens TJ, Ritsema J (1999) The TauP Toolkit: Flexible seismic travel-time and ray-path utilities. Seismol Res Lett 70: 154–160

Diehl T, Ritter JRR (2005) The crustal structure beneath SE Romania from teleseismic receiver functions. Geophys J Int 163: 238-251

Fan G, Wallace TC, Zhao D (1998) Tomographic imaging of deep velocity structure beneath the Eastern and Southern Carpathians, Romania: implications for continental collision. J Geophys Res 1023: 2705-2723

Fillerup MA, Knapp JH, Knapp, CC, Raileanu V (2010) Mantle earthquakes in the absence of subduction? Continental delamination in the Romanian Carpathians. Lithosphere 2:333-340 doi: 10.1130/L102.1

Geissler WH, Kind R, Yuan X (2008) Upper mantle and lithospheric heterogeneities in central and eastern Europe as observed by teleseismic receiver functions. Geophys J Int 174: 351-376

Gîrbacea R, Frisch W (1998) Slab in the wrong place: lower lithospheric mantle delamination in the last stage of the Eastern Carpathian subduction retreat. Geology 26: 611-614

Gvirtzman Z (2002) Partial detachment of a lithospheric root under the southeast Carpathians: toward a better definition of the detachment concept. Geology 30: 51-54

Hauser F, Raileanu V, Fielitz W, Bala A, Prodehl C, Polonic G, Schulze A (2001) VRANCEA99–the crustal structure beneath southeastern Carpathians and Moesian Platform from a seismic refraction profile in Romania. Tectonophysics 340: 233-256

Hauser F, Raileanu V, Fielitz W, Dinu C, Landes M, Bala A, Prodehl C (2007) Seismic crustal structure between the Transylvanian Basin and the Black Sea, Romania. Tectonophysics 430: 1–25

International Seismological Centre, On-line Bulletin, http://www.isc.ac.uk, Internatl. Seis. Cent., Thatcham, United Kingdom, 2001.

Ivan M (2007) Attenuation of P and pP waves in Vrancea area – Romania. J Seismol. doi:10.1007/s10950-006-9038-7

Knapp HJ, Knapp CC, Raileanu V, Matenco L, Mocanu V, Dinu C (2005) Crustal constraints on the origin of mantle seismicity in the Vrancea Zone, Romania: the case for active continental delamination. Tectonophysics 410: 311–323

Milsom J (2005) The Vrancea seismic zone and its analogue in the Banda Arc, eastern Indonesia. Tectonophysics 410: 325-336

Mucuta DM, Knapp CC, Knapp JH (2006) Constraints from Moho geometry and crustal thickness on the geodynamic origin of the Vrancea Seismogenic Zone (Romania). Tectonophysics 420: 23-36

Nakamura M, Ando M, Ohkura T (1998) Fine structure of deep Wadati-Benioff zone in the Izu-Bonin region estimated from S-to-P converted phase. Phys Earth planet Inter 106: 63-74

Narcía-López C, Castro RR, Rebollar CJ (2004) Determination of crustal thickness benetah Chiapas, Mexico using S and Sp waves. Geophys J Int 157: 215-228

Oczlon MS (2006) Terrane Map of Europe, 1st edition. Gaea Hedelbergensis 15

Ohmi S, Hori S (2000) Seismic wave conversion near the upper boundary of the Pacific plate beneath the Kanto district, Japan. Geophys J Int 141: 136-148

Oncescu MC (1984) Deep structure of Vrancea region, Romania, inferred from simultaneous inversion for hypocenters and 3-D velocity structure. Ann Geophysicae 2: 23-28

Oncescu MC, Marza VI, Rizescu M, Popa M (1999) The Romanian Earthquake Catalogue between 984-1997. In: Vrancea Earthquakes: Tectonics, Hazard and Risk Mitigation, Wenzel F, Lungu D (eds.) and Novak O (co-ed), pp 43-47, Kluwer Academic Publishers, Dordrecht, Netherlands.

Polonic G (1996) Structure of the crystalline basement in Romania. Rev Roum Geophys 40: 57-71

Regnier M, Chiu, J-M, Smalley Jr R, Isacks BL, Araujo M (1994) Crustal Thickness Variation in the Andean Foreland, Argentina, from Converted Waves. Bull Seism Soc Am 84: 1097-1111

Raykova RB, Panza GF (2006) Surface waves tomography and non-linear inversion in the the southeast Carpathians. Phys Earth planet Inter 157: 164-180

Romanian Quasi-geoid Map, scale 1:1,000,000. Military Topographic Department, Romanian Ministry of Defense

Sacks IS, Snoke JA (1977) The use of converted phases to infer the depth of the lithosphere-astenosphere boundary beneath South America. J Geophys Res 82: 2011-2017

Smith WD (1970) S to P Conversions as an aid to crustal studies. Geophys JR astr Soc 19: 513-519

Sperner B, Lorentz F, Bonjer K-P, Hettel S, Müller B, Wenzel F (2001) Slab break-off – abrupt cut or gradual detachment ? New insights from Vrancea region (SE-Carpathians, Romania). Terra Nova 13: 172-179

Tãtaru D (2009) Research on lithosphere structure in Romania by using receiver functions method (in Romanian). Ph.D. thesis, University of Bucharest

Wang R (1999) A simple orthonormalization method for the stable and efficient computation of Green's functions. Bull Seism Soc Am 89: 733-741

Wessel P, Smith WHF (1996) A global, self-consistent, hierarchical, high-resolution shoreline database. J Geophys Res 101: 8741-8743

Zhu L, Kanamori H (2000) Moho depth variation in southern California from teleseismic receiver functions. J Geophys Res 105: 2969-2980

Fig. 1 Main tectonic settings of Vrancea and adjacent area (simplified after Polonic (1996) and Oczlon (2006). Crosses indicate the epicenters of the intermediate depth events used in this study. A histogram of the focal depths is also presented. North, Central and South Dobrogea regions are indicated by ND, CD and SD, respectively. Shot points of previous seismic refraction lines are indicated by circles (VRANCEA99) and squares (VRANCEA2001) experiments. Diamonds show the location of some CALIXTO99 temporary stations. C-O Fault and P-C Fault are Peceneaga-Camena and Capidava-Ovidiu crustal faults, respectively.

Fig. 2 Location of the permanent seismological stations used in this study. The inset is a histogram of the earthquake magnitudes. The background is a simplified version (astronomic values only) of the quasi-geoid heights (according to the Romanian Quasi-Geoid Map, scale 1:1,000,000, Military Topographic Department).

Fig 3. (a) Recording at MLR station (Δ=0.3°, STS-2 instrument) of the 2005/04/04 Vrancea event (18:59:04.2 UT, 45.42N, 26.36E, 141 km depth, Mw=4.1). Note the conspicuous phase between P and S, interpreted as a S converted to P on Moho. The inset shows the focal mechanism obtained from polarities of the first arrivals. Note the position of MLR station in the proximity of a nodal plane. For the same event, the converted phase has been also observed with a good quality at BUC1 (same location as BMG in Table 1) and SUL and fairly at AMR, FUL and SEC. Poor quality phase have been recorded at OZU, PGO and IASI (at the last station, because of the high noise level). O-C values are indicated in a parenthesis.

Fig. 4 Theoretical arrival time difference sp-p for hypocenter depths at 130, 140 and 150 km. Note the three curves are near parallel ones. The inset shows the sp and p paths for an event at 140 km depth recorded at an epicentral distance of 1°. The local velocity model routinely used in Vrancea earthquake location has been used (Oncescu 1984).

Fig 5. Moho depths versus t_j values at the representative stations. Note the linear regression with the R-squared parameter close to the unit.

Fig 6. Temporary stations of CALIXTO experiment with observed converted phases (diamonds) and RF analysis (Diehl, 2005)(circles).

Fig. 7. Moho depth estimations in Vrancea and adjacent area. Piercing points to Moho of sp and p waves are indicated by circles and squares, respectively. Figures indicate the average values of Moho depth obtained by Raykova and Panza (2006) in a cell grid of 1° x 1°.

Fig.8. Vertical component recordings of 2005/04/04 event (see Fig.3), aligned to the direct P arrivals. Converted sp phases (manually picked) are indicated by vertical bars. Computed sp arrivals for the LVM with the Moho depth at 40 km are indicated by arrows (for focal depth h=141 km) and by diamonds (for h=121 km). Triangles shown the sp arrivals for the variable Moho depth model and h=121 km.

Table 1 Coordinates of the used stations, the number of sp/p phases observed at each station, average earthquakes and t_j values (with standard errors). Representative stations for a certain group are bolded.

Table 2 Comparison of Moho depth obtained in this study with some previous results. Z & K abbreviates Zhu and Kanamori (2000) method.

colour figure1

Click here to download high resolution image

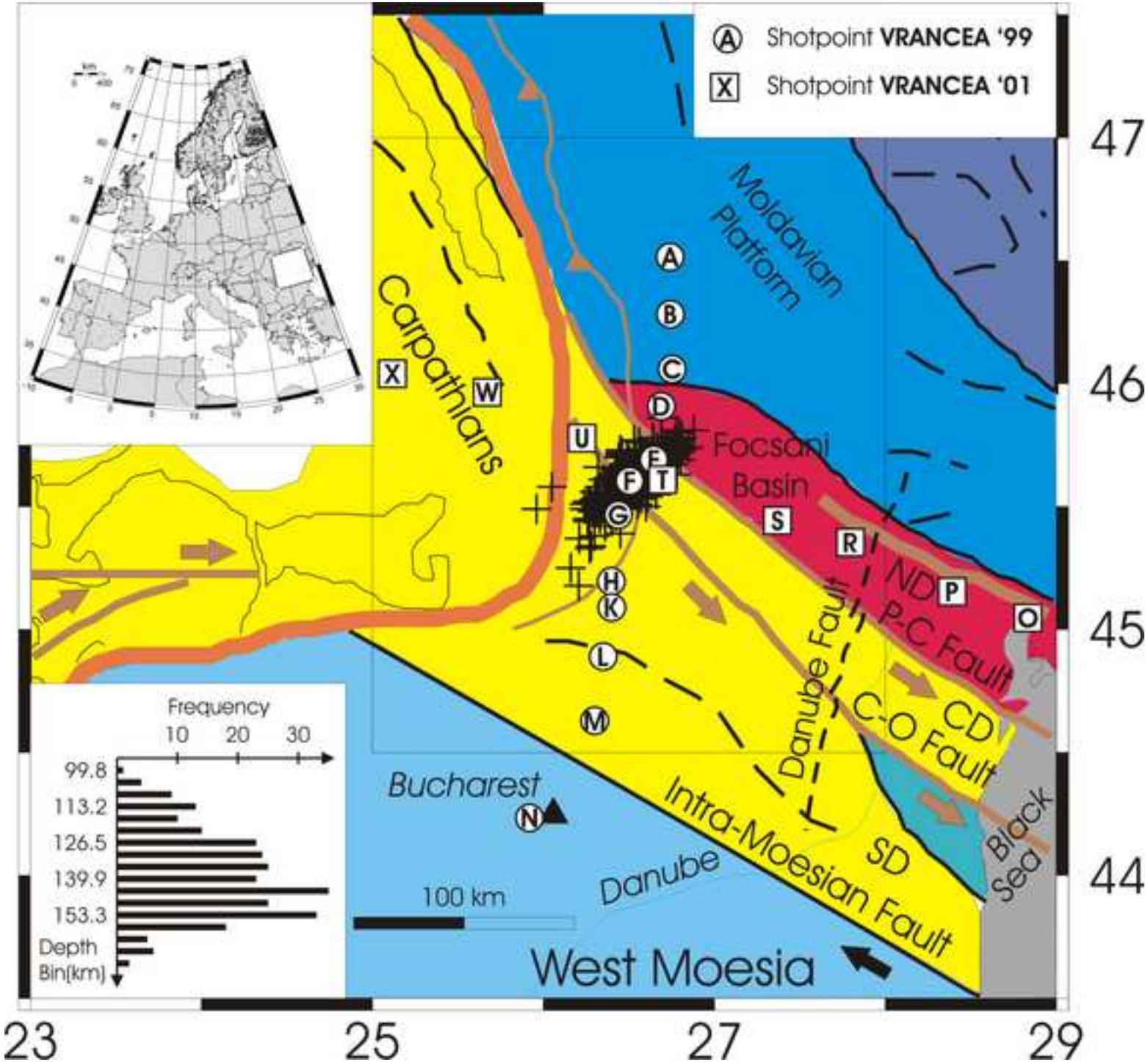

colour figure2

Click here to download high resolution image

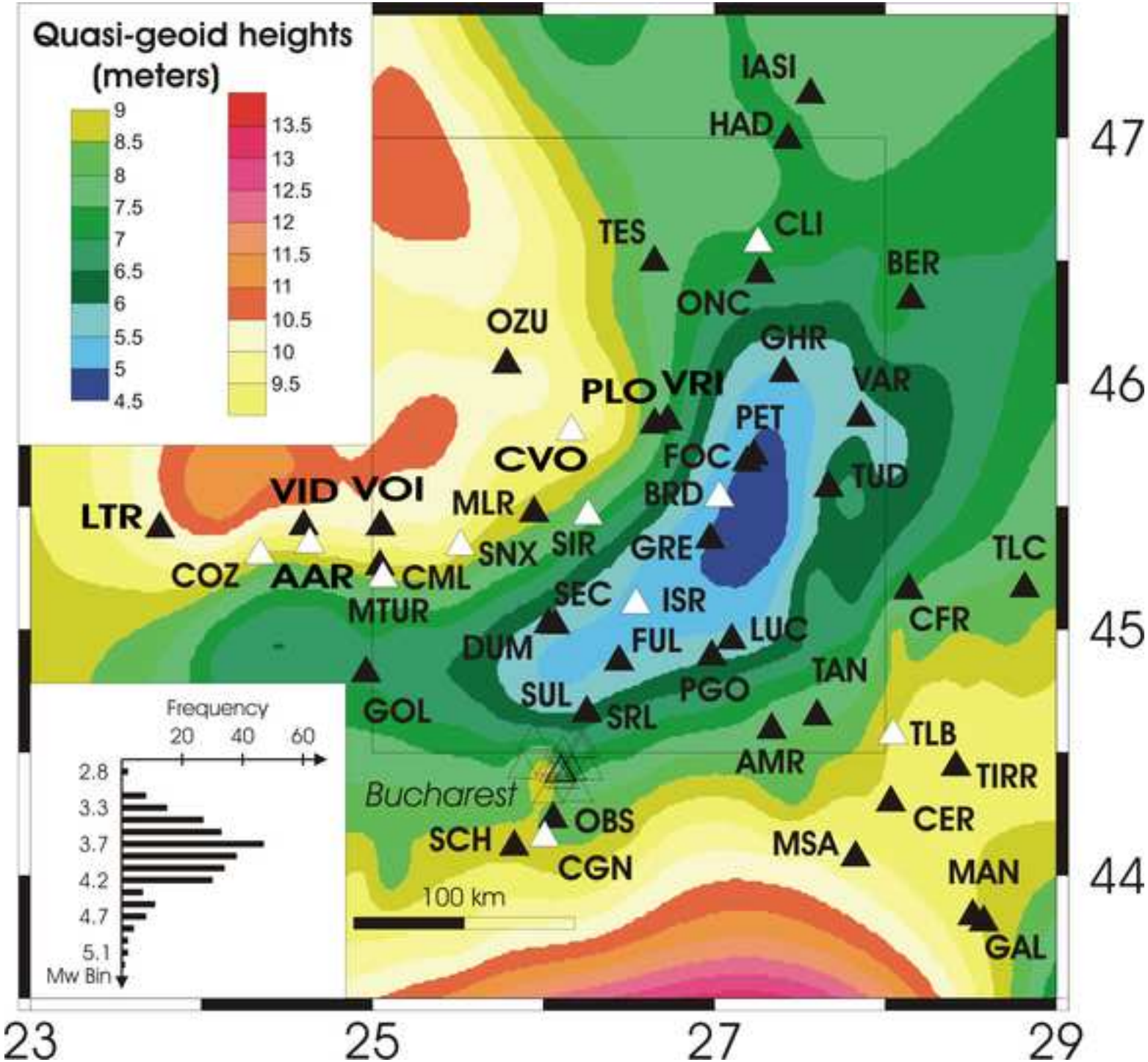

line figure1

Click here to download high resolution image

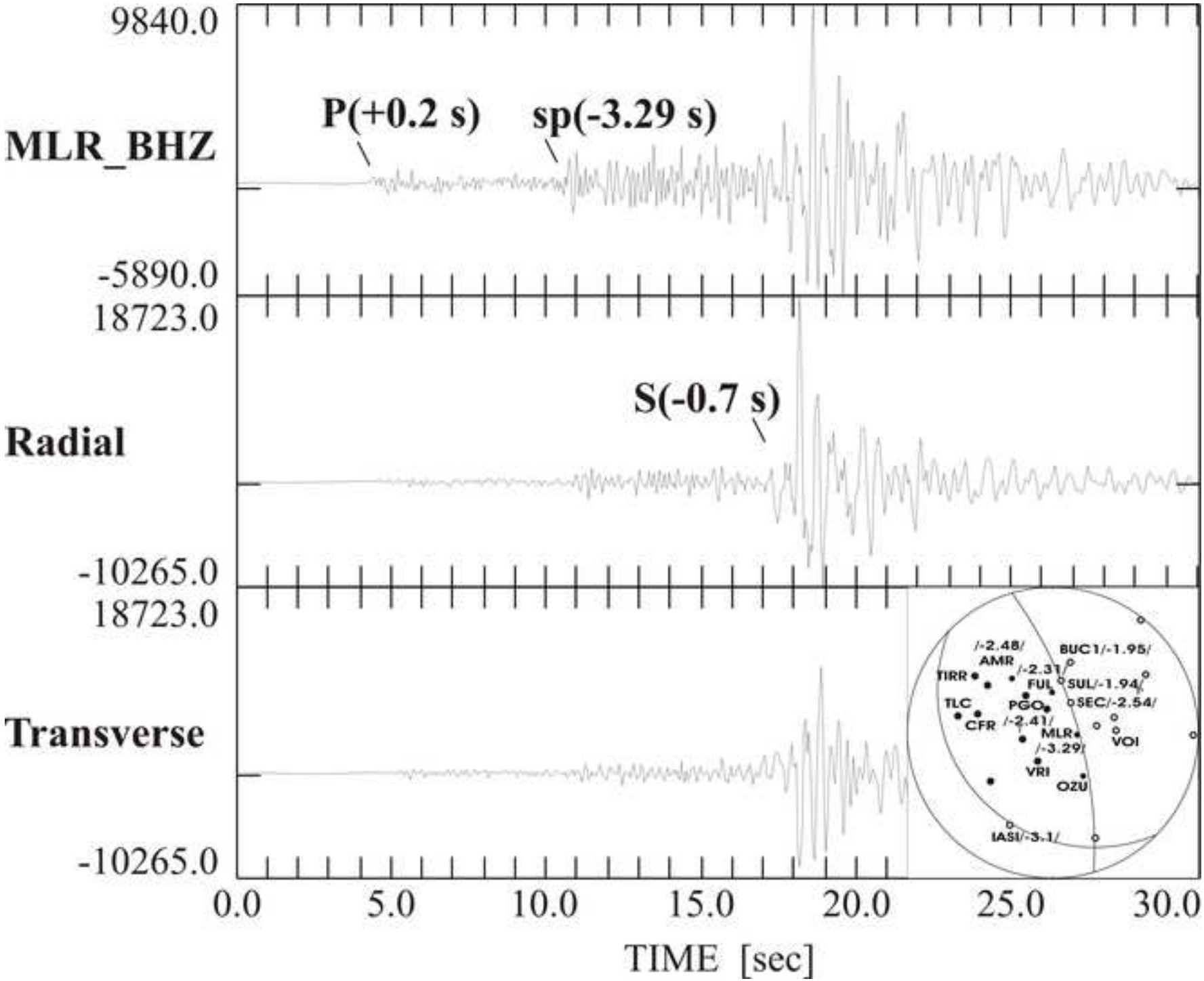

line figure2
Click here to download high resolution image

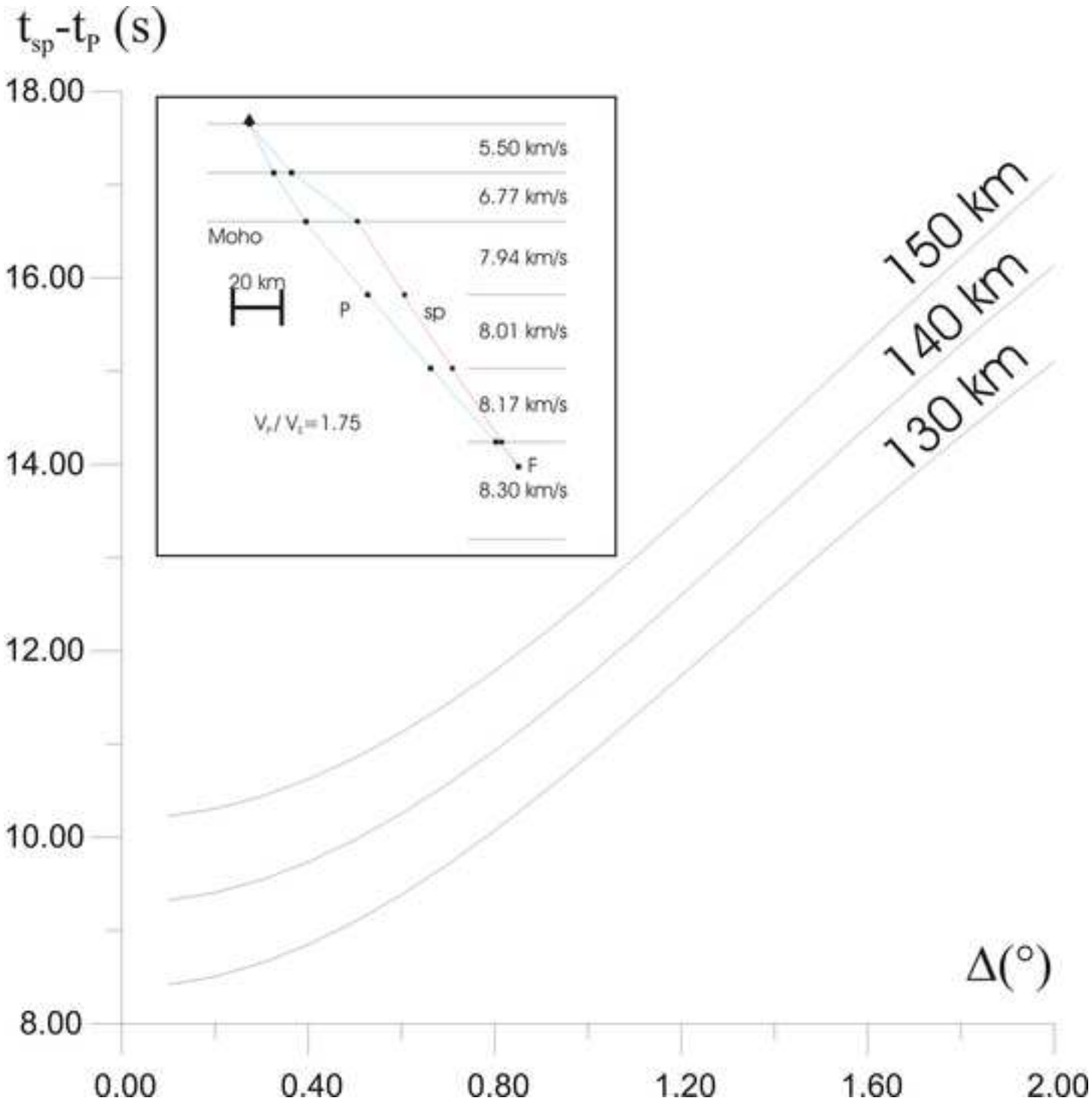

line figure3
Click here to download high resolution image

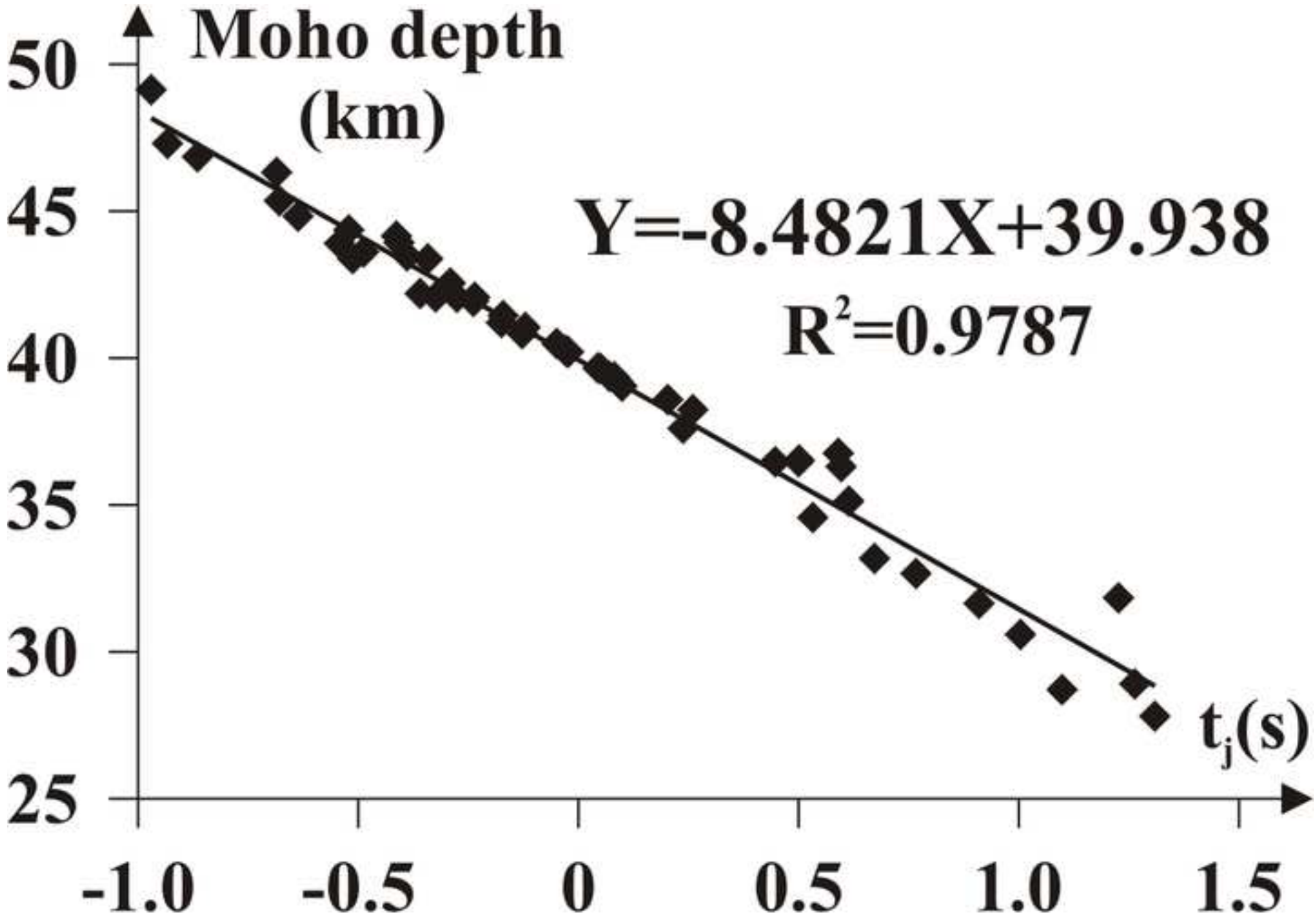

line figure4

Click here to download high resolution image

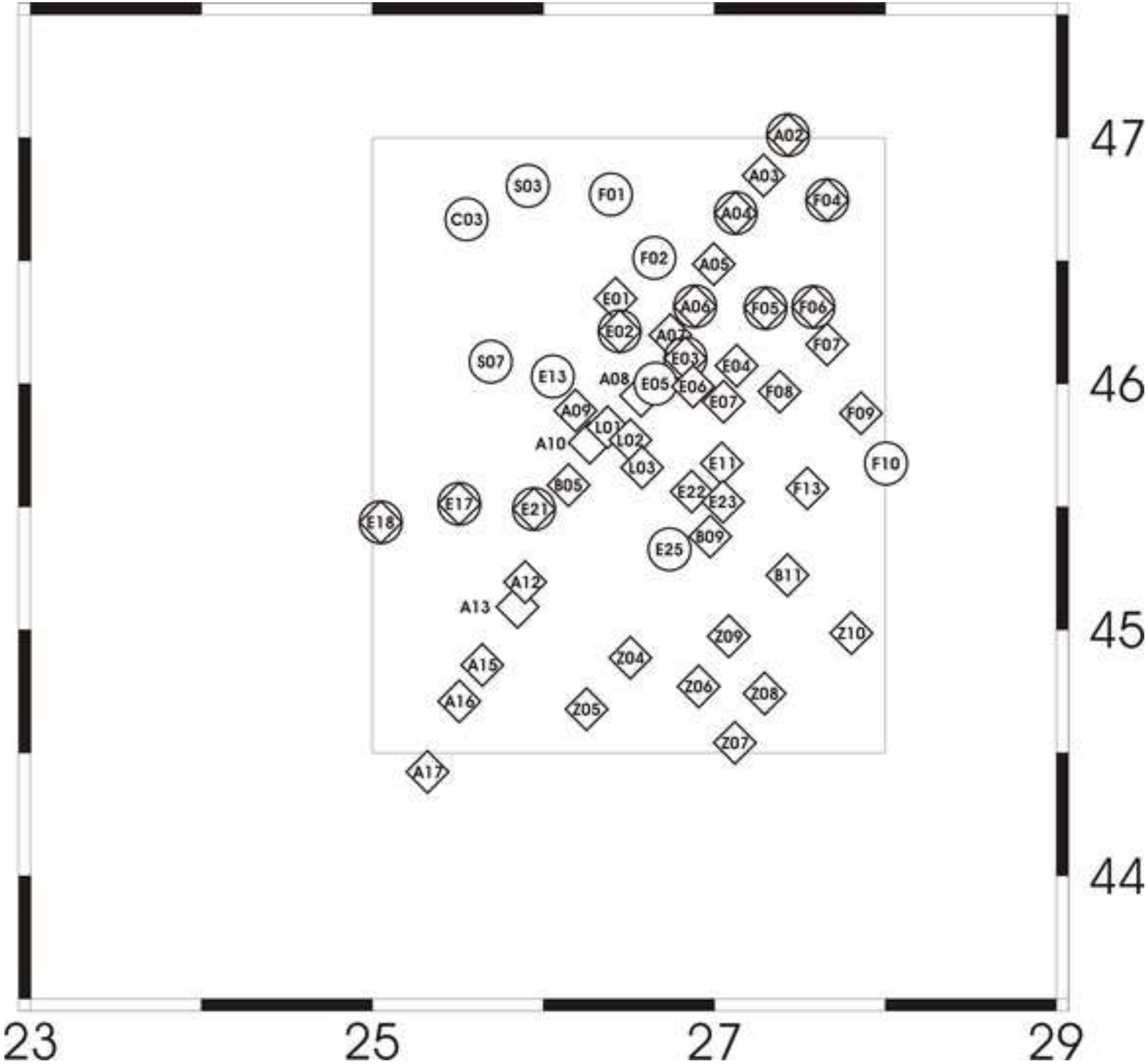

colour figure3
Click here to download high resolution image

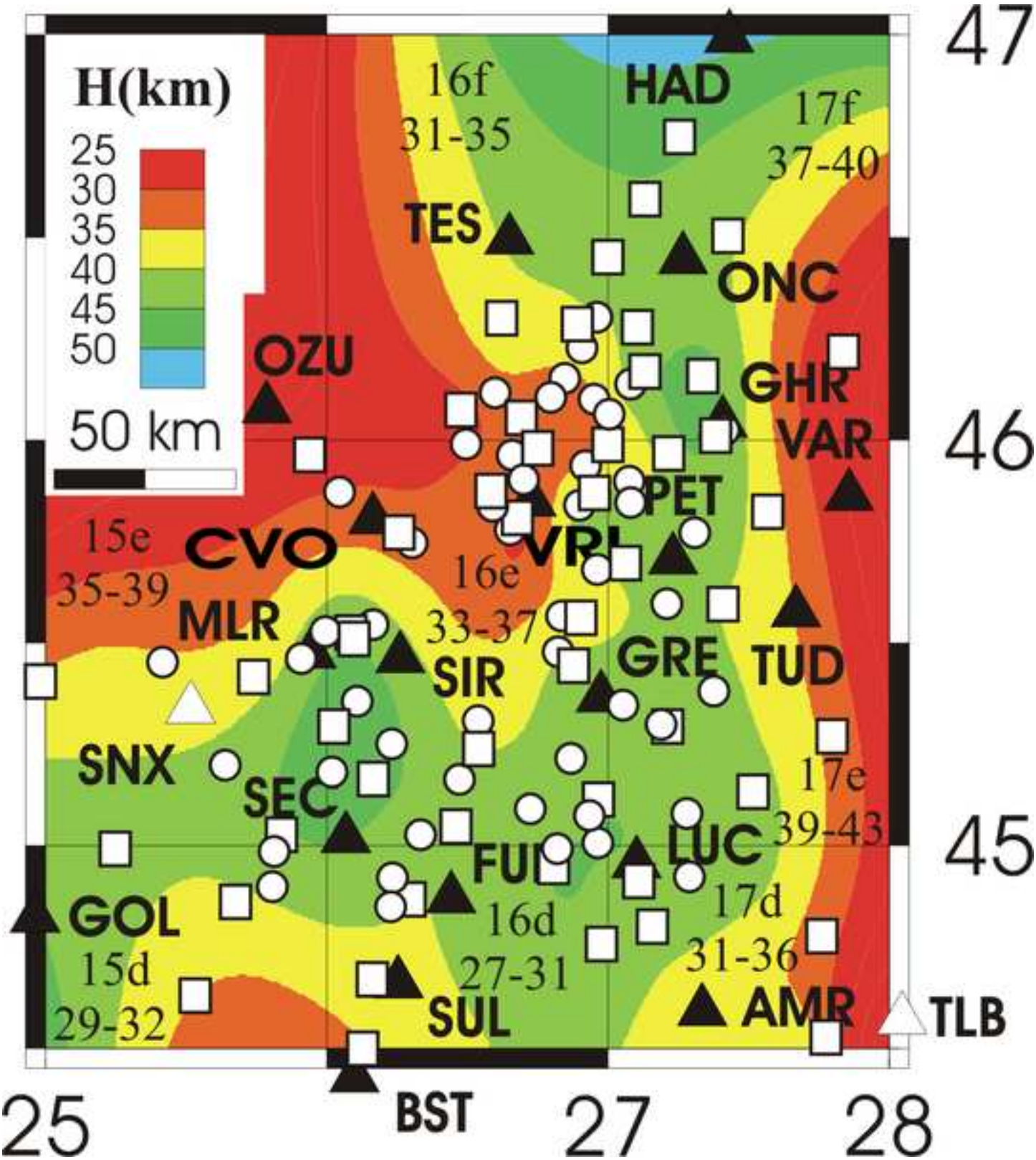

colour figure4

Click here to download high resolution image

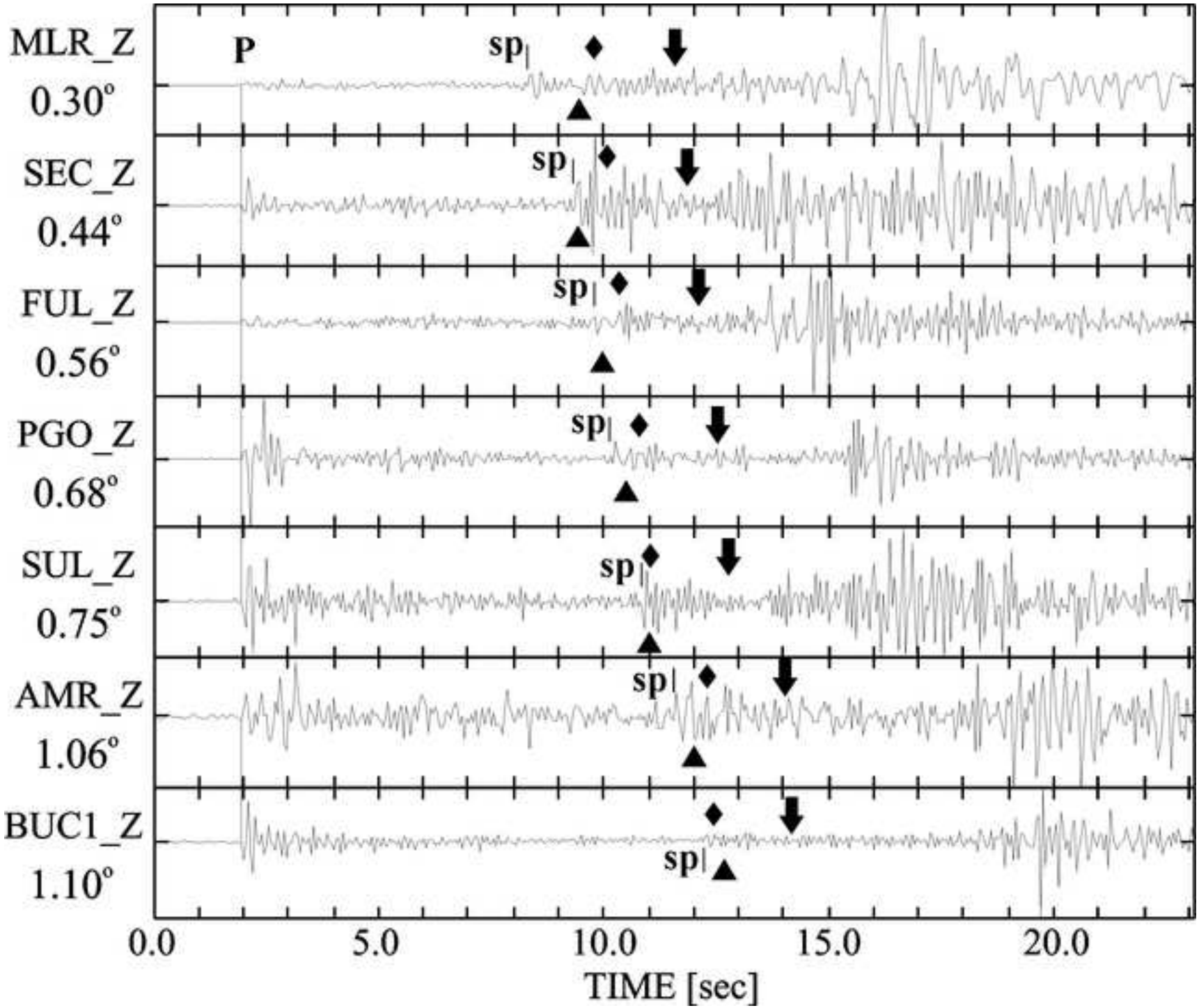

table1

Click here to download table: Tabel1.doc

Station	No.pha.	Lat [°N]	Lon [°E]	Elev. (m)	Average earthquake			t_j (s) (±st. err.)
					Lat [°N]	Lon [°E]	Depth (km)	
AAR	2	45.3656	24.6332	912	45.5537	26.3969	137.57	0.50 (±0.12)
CML	1	45.2747	25.0439	557				
COZ	3	45.3205	24.3425	1610				
LTR	4	45.4284	23.7585	1418				
MTU	10	45.2261	25.063	1018				
VID	1	45.4379	24.5985	876				
VOI	9	45.4371	25.0496	1030				
E18	2	45.437	25.049	970				
SUL	66	44.6777	26.2526	128	45.5832	26.4638	140.48	-0.02 (±0.03)
AFU	1	44.5338	26.2366	124				
MOG	3	44.5649	25.9417	145				
PIP	1	44.5137	26.1143	129				
SRL	2	44.6786	26.2551	73				
STF	2	44.5324	26.2131	124				
Z05	2	44.6775	26.2527	166				
AMR	35	44.6103	27.3354	67	45.5669	26.4283	141.02	-0.28 (±0.04)
TAN	1	44.6656	27.6025	85				
BST	11	44.4457	26.0984	126	45.6066	26.4327	144.01	0.04 (±0.03)
BAP	2	44.4059	26.1190	105				
BBI	7	44.4411	26.1618	116				
BCU	3	44.4107	26.0938	95				
BDL	4	44.4658	26.0696	135				
BFG	6	44.4386	26.1011	75				
BGM	16	44.4562	26.0850	325				
BHM	5	44.4351	26.1023	125				
BIS	2	44.4370	26.1067	136				
BLH	5	44.4525	26.1123	149				
BOT	11	44.4366	26.0653	76				
BPF	8	44.4672	26.0467	14				
BTM	7	44.4371	26.1067	142				
BVC	11	44.4301	26.1017	111				
CIO	7	44.4489	25.8799	138				
CNC	5	44.4439	26.2619	106				
IBA	9	44.4409	26.1624	109				
INB	14	44.4408	26.1611	109				
IRO	7	44.4409	26.1624	109				
RBA	4	44.4409	26.1624	114				
RRO	5	44.4401	26.1624	114				

BER	19	46.3589	28.1501	63	45.6137	26.5321	139.94	1.23 (±0.10)
OBS	1	44.2470	26.0569	115	45.6062	26.4463	143.85	0.26 (±0.05)
BMG	19	44.3479	26.0281	120				
CGN	5	44.1712	26.0067	78				
POP	2	44.3554	26.2034	109				
SCH	29	44.1345	25.8294	109				
CER	2	44.3145	28.0326	82	45.59	26.45	151.1	0.60 (±0.19)
MSA	1	44.0910	27.8256	106				
TIRR	4	44.4581	28.4128	77				
CFR	21	45.1781	28.1363	52	45.6054	26.5075	130.55	0.20 (±0.18)
TLC	3	45.1856	28.8149	50				
CVO	12	45.8224	26.1646	442	45.6193	26.5357	130.15	0.67 (±0.10)
A09	1	45.8912	26.1882	596				
A10	1	45.7603	26.2707	1026				
B05	4	45.5882	26.1475	674				
L01	1	45.8233	26.375	1759				
L02	3	45.7712	26.5088	1103				
L03	1	45.6597	26.5778	369				
SEC	60	45.0355	26.0676	417	45.6269	26.5192	140.73	-0.69 (±0.03)
DUM	1	45.0383	26.0316	250				
PET	44	45.7230	27.2317	109	45.6049	26.4855	137.87	-0.02 (±0.07)
FOC	2	45.6975	27.1922	78				
E11	1	45.6765	27.0435	345				
FUL	64	44.8877	26.4424	117	45.6224	26.5213	137.88	-0.39 (±0.02)
Z04	11	44.8865	26.5087	98				
MAN	2	43.8529	28.5109	94	45.5467	26.3933	136.83	0.59 (±1.81)
GAL	1	43.8275	28.5752	56				
GHR	44	46.0605	27.4080	213	45.6247	26.5218	139.35	0.09 (±0.05)
F08	1	45.9682	27.3817	133				
GOL	14	44.8399	24.9630	299	45.655	26.5221	144.54	-0.17 (±0.11)
GRE	20	45.3834	26.9744	191	45.6509	26.5429	139.49	-0.05 (±0.06)
B09	1	45.3792	26.9757	247				
HAD	26	47.0103	27.4307	403	45.6303	26.5248	133.84	-0.51 (±0.07)
IAS	3	47.1933	27.5550	160				
A02	2	47.0108	27.4305	414				
LUC	39	44.9739	27.1011	120	45.6067	26.483	136.8	-0.29 (±0.03)
PGO	15	44.9080	26.9846	100				
Z09	8	44.9738	27.0843	63				

MLR	64	45.4912	25.9456	1392	45.6385	26.5514	136.61	-0.34 (±0.06)
E21	1	45.491	25.945	1361				
ONC	20	46.4643	27.2672	233	45.6016	26.5228	132.91	0.08 (±0.04)
CLI	37	46.5888	27.2562	502				
OZU	10	46.0958	25.7866	663	45.532	26.433	130.36	1.26 (±0.10)
VRI	68	45.8657	26.7277	475	45.6181	26.5128	137.78	1.10 (±0.05)
PLO	10	45.8512	26.6499	656				
SIR	18	45.4801	26.2617	512	45.6122	25.5161	139.96	-0.41 (±0.08)
TES	29	46.5118	26.6489	372	45.6131	26.5352	124.34	0.45 (±0.06)
TLB	36	44.5888	28.0452	60	45.5772	26.4827	136.65	-0.32 (±0.05)
TUD	46	45.5933	27.6687	163	45.5981	26.4932	135.44	-0.03 (±0.11)
F13	1	45.575	27.5432	59				
VAR	45	45.8802	27.8569	195	45.6091	26.5134	135.86	-0.24 (±0.10)
F09	2	45.8803	27.8573	222				
SNX	6	45.3553	25.5155	1470	45.6312	26.5525	137.6	0.07 (±0.11)
E17	2	45.5122	25.5082	1036				
A15	2	44.857	25.6428	225	45.595	26.505	126.85	-0.86 (±0.03)
Z06	8	44.77	26.9085	93	45.5563	26.4512	131.75	-0.52 (±0.07)
Z07	8	44.5408	27.1202	50	45.5438	26.4462	130.2	-0.64 (±0.03)
A03	4	46.8468	27.2878	230	45.6025	26.5325	129.6	-0.13 (±0.12)
A04	4	46.6938	27.1253	239	45.565	26.55	126.92	0.05 (±0.09)
A07	5	46.1978	26.7425	276	45.595	26.53	129.98	0.91 (±0.07)
A06	1	46.3148	26.8875	421				
A12	3	45.1942	25.8933	447	45.635	26.4825	137.65	-0.97 (±0.13)
A13	1	45.0937	25.8488	402				
A17	2	44.4223	25.3222	188	45.465	26.395	136.25	0.50 (±0.03)
E02	4	46.2132	26.4462	494	45.65	26.57	127.42	1.31 (±0.14)
E01	1	46.3462	26.4223	438				
F04	3	46.7468	27.6595	265	45.6133	26.5933	121.37	-0.36 (±0.97)
B11	3	45.2223	27.4272	88	45.5533	26.4167	140.5	-0.24 (±0.34)
E04	4	46.0733	27.1303	227	45.6975	26.555	137.97	0.77 (±0.16)
F05	6	46.3073	27.2993	222	45.6933	26.5617	132.97	-0.12 (±0.13)
A05	5	46.4862	26.9967	187	45.594	26.532	129.7	0.61 (±0.06)
E03	5	46.1033	26.8308	370	45.5838	26.4937	130.45	1.00 (±0.17)
E06	1	45.989	26.8752	335				
E07	5	45.9273	27.0538	314	45.694	26.642	129.38	-0.41 (±0.36)
F06	2	46.3122	27.5788	141	45.675	26.59	119.8	-0.93 (±0.05)
Z08	5	44.7413	27.2942	66	45.528	26.434	132.38	-0.68 (±0.11)
A16	2	44.7093	25.5083	220	45.39	26.265	132.95	-0.17 (±0.12)

BRD	10	45.5533	27.03	356	45.5875	26.4975	133.51	0.24 (±0.08)
E22	1	45.5618	26.867	362				
E23	1	45.5205	27.0502	275				
F07	2	46.16	27.6592	130	45.46	26.385	130.6	-0.49 (±0.28)
A08	5	45.9518	26.572	632	45.6806	26.6144	114.48	0.53 (±0.19)
Z10	2	44.9865	27.8013	55	45.645	26.495	126	-0.54 (±0.78)
ISR	12	45.1188	26.5431	750	45.6425	26.53	137.57	0.10 (±0.17)

table2
Click here to download table: Tabel2.doc

This study: Nearest grid point coordinates			Receiver function					Obs.
Lat. [°N]	Lon [°E]	H [km]	Station	Lat. [°N]	Lon [°E]	Bootstrap H [km]	Chi-Square H [km]	
46.313	26.879	39.3	A06	46.3148	26.887	38.4±5.3	37.1±0.9	CALIXTO99 Diehl et al. (2005)
46.219	26.455	32.5	E02	46.2132	26.446	31.3±1.7	31.5±1.0	
46.094	26.818	32.5	E03	46.1033	26.831	35.8±1.4	35.7±1.0	
46.0	26.667	31.7	E05	46.0002	26.656	32.4±3.4	31.2±1.0	
46.031	26.061	27	E13	46.0297	26.055	31.7±4.5	34.0±1.0	
45.5	25.515	34.6	E17	45.5122	25.508	38.1±3.6	39.0±1.4	
45.438	25.061	35.5	E18	45.437	25.049	35.3±3.2	35.4±1.3	
45.5	25.939	42	E21	45.491	25.945	45.0±1.6	45.5±1.1	
45.313	26.727	40.1	E25	45.3272	26.738	30.4±1.7	31.0±0.9	
46.781	26.394	38.2	F01	46.7698	26.395	38.0±3.7	38.5±0.9	
45.5	26.636	40.3	F02	46.5117	26.649	37.3±5.9	34.9±1.1	
46.75	27.667	41.4	F04	46.7468	27.66	34.4±2.0	34.9±1.2	
46.313	27.303	42.7	F05	46.3073	27.299	43.2±4.2	40.6±1.5	
46.313	27.576	35.6	F06	46.3122	27.579	37.2±5.1	33.6±0.9	
46.094	25.697	23.3	S07	46.0903	25.692	27.6±1.5	27.4±1.1	
45.5	25.939	42	MLR	45.4920	25.946	45.1±1.4	45.0±1.5	
			Receiver function					
			Station	Lat. [°N]	Lon [°E]	H [km]		Geissler et al. (2008)
			MLR	45.4920	25.946	45		
45.875	26.727	30.9	VRI	45.866	26.728	28(46)		
			Receiver function					
			Station	Lat. [°N]	Lon [°E]	Ps conversion H [km]	Z & K H [km]	Tãtaru (2009)
			VRI / PLO			32±1	-	
			MLR			32 / 44	32±1	
46.531	26.667	40.9	TES	46.5188	26.6489	36±1	-	
45.719	27.242	41.5	PET	45.723	27.2311	44±2	42±1	
			Seismic refraction profiles					
			Shotpoint	Lat. [°N]	Lon [°E]	H [km]		VRANCEA99 VRANCEA01
45.906	26.697	30.8	D	45.908	26.69	39.7		

45.688	26.636	30.6	E	45.691	26.646	40.7	Hauser et al. (2001) Hauser et al. (2007)
45.594	26.515	33.6	F	45.604	26.505	41	
45.469	26.424	37.6	G	45.466	26.439	41	
45.188	26.394	43.1	H	45.196	26.397	41	
45.094	26.394	43.5	K	45.09	26.4	41	
44.875	26.364	40.1	L	44.89	26.35	41	
44.625	26.303	38.3	M	44.629	26.3	39	
45.344	27.8182	33.1	R	45.354	27.796	44.4	
45.438	27.364	40.9	S	45.443	27.369	45.1	
45.625	26.697	32.6	T	45.609	26.697	43.9	
45.781	26.212	32.8	U	45.778	26.226	33.4	
45.969	26.667	25.3	W	45.965	25.672	34.5	